ADVANCED QUANTUM TECHNOLOGIES
www.advquantumtech.com

Coupling Nanostructured CsNiCr Prussian Blue Analogue to Resonant Microwave Fields

Alberto Ghirri, Christian Herrero, Sandra Mazérat, Talal Mallah, Oscar Moze, and Marco Affronte*

Collective spin excitations in magnetically ordered materials are exploited for advanced applications in magnonics and spintronics. In these contexts, conditions for minimizing dissipative effects are sought in order to obtain long living excitations that can be coherently manipulated. Organic and coordination materials may offer alternative options for their flexibility and low spin–orbit effects. Likewise, ferromagnetic nanostructures provide a versatile platform for hybrid architectures, yet downsizing affects the spin dynamics and needs to be controlled. Here, a systematic investigation on insulating $CsNiCr(CN)_6$ Prussian blue analogue, including isolated nanoparticles dispersed in polyvinylpyrrolidone, mutually interacting nanoparticles embedded in cetyltrimethylammonium, and bulk samples, is reported. Ferromagnetic resonance spectroscopy is performed in a wide temperature range across the bulk ferromagnetic transition occurring at 90 K. This allows us to monitor key parameters through different types of nanostructured samples. It is found that the Gilbert damping parameter of 10 nm nanoparticles compares well (10^{-3}) with values reported for prototypical yttrium iron garnet $Y_3Fe_5O_{12}$. Strong coupling with the microwave field of a microstrip resonator is then observed for bulk $CsNiCr(CN)_6$ as well as for interacting nanoparticles. These results clarify conditions for the coherent manipulation of collective spin degrees of freedom in nanostructured coordination materials.

In a single domain magnetically ordered material, the fast dynamics of the magnetization is described as precession around an effective magnetic field damped by magnetic viscosity. Under the excitation of electromagnetic (micro)wave, nutation and energy exchange occurs at resonance, as evidenced in ferromagnetic resonance (FMR) experiments. Magnetic materials with low damping are now attracting much interest for their use in spintronics and magnonics since they allow generation and propagation of magnons (i.e., spin excitations of quasistatic magnetization) with low dissipation. For instance, spin pumping at the interface between a ferromagnet and normal metal has been proved as an efficient method to generate a spin current,[1] materials with long living spin waves are used in spin caloritronics[2,3] while controlled interference of spin waves are currently being investigated for non-boolean logic devices operating with low power consumption.[4,5] In particular conditions, that is, when the coupling with electromagnetic radiation becomes stronger than damping, coherent dynamics of the magnetization and photons occurs thus allowing the realization of hybrid circuits in which the transfer of magnetic excitations to microwaves takes place with high fidelity[6] and eventually in the quantum regime, that is, when few excitations are involved.[7]

In these research areas, yttrium iron garnet $Y_3Fe_5O_{12}$ (YIG in short)[8,9] is considered the reference inorganic (ferri)magnetically ordered material for its low damping coefficient, yet its performance critically depends on the size and shape of the specimen. In search of alternative materials to be grown on different substrates and possibly to be scaled up/down in size, high performances, that is, sharp resonance linewidth, have been recently reported in organic-based ferrimagnetic vanadium tetracyanoethylene thin films.[10] Prussian blue analogues (PBA) are characterized by cyanide coordination ligands and Heisenberg exchange coupling between transition metal spins.[11] FMR spectroscopy has been reported for a few PBA compounds.[12–14] Here, we consider the $CsNi^{II}Cr^{III}(CN)_6$ derivative (CsNiCr in short) which has a face-centered cubic unit cell. Ferromagnetic exchange coupling between the Ni and the Cr sublattices induces magnetic order at Curie temperature T_C(bulk) = 90 K.[11,15] Isolated CsNiCr nanoparticles (NPs) dispersed in polyvinylpyrrolidone (PVP) organic polymer have been synthesized with a narrow

Dr. A. Ghirri, Prof. M. Affronte
Istituto Nanoscienze – CNR
via Campi 213/a, 41125 Modena, Italy
E-mail: alberto.ghirri@nano.cnr.it
Dr. C. Herrero, S. Mazérat, Prof. T. Mallah
Institut de Chimie Moléculaire et des Matériaux d'Orsay
CNRS
Université Paris Sud, Université Paris Saclay
91405 Orsay, France
Prof. O. Moze, Prof. M. Affronte
Dipartimento di Scienze Fisiche, Informatica e Matematica
Università di Modena e Reggio Emilia
via Campi 213/a, 41125 Modena, Italy
The ORCID identification number(s) for the author(s) of this article can be found under https://doi.org/10.1002/qute.201900101

DOI: 10.1002/qute.201900101

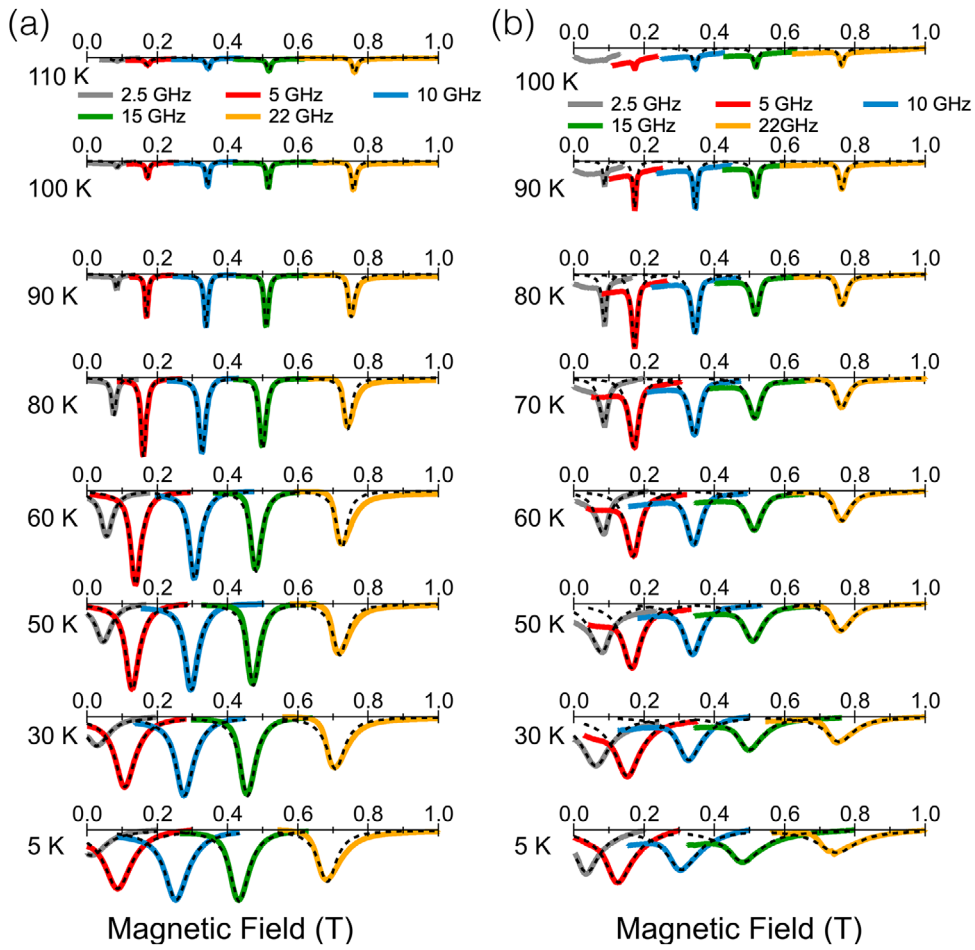

Figure 1. Transmission spectra measured at different frequency and temperature for a) bulk CsNiCr and b) 10 nm NPs dispersed in PVP polymer. Dashed lines show the fit with a Lorentzian lineshape.

size distribution.[16,17] Effects of inter-particle coupling are not evident for CsNiCr nanoparticles highly diluted in PVP matrix. Conversely, dispersion in cetyltrimethylammonium (CTA^+) matrix is not effective to magnetically decouple CsNiCr nanoparticles.[18] Indeed, in the latter case, magnetometry and small angle neutron scattering (SANS) experiments evidenced the presence of sizeable inter-particle interactions with magnetic correlation lengths estimated to be (12 ± 4) nm for 8.6 nm NPs and (40 ± 20) nm for 4.8 nm NPs.[19]

We first performed broadband FMR spectroscopy in the 1–26 GHz frequency (ω) range by means of a microstrip transmission line to identify the main features of the absorption spectra. This study was systematically performed on three types of samples: bulk, NPs diluted in PVP polymer, and NPs embedded in a CTA^+ matrix. Moreover, three (two) sizes of NPs [6, 8 and, 10 nm (4.8 and 8.6 nm)] dispersed in PVP (CTA^+) were investigated in order to evaluate size effects on FMR spectra.

Figure 1a shows FMR spectra taken on a bulk sample of CsNiCr. A faint FMR absorption dip is visible above T_C (110 K), which becomes well pronounced at the Curie temperature (T_C = 90 K). For lower temperatures ($T < 60$ K) and for each frequency of excitation, the absorption dip gets smaller and the resonance line broadens. The position of the FMR line linearly scales with the frequency ω while the resonance field progressively shifts to lower magnetic field values as temperature decreases. A qualitatively similar behavior is observed in nanostructured samples: Figure 1b shows the evolution of FMR spectra for 10 nm CsNiCr NPs dispersed in PVP polymer for direct comparison with bulk behavior. Some differences with respect to the bulk behavior can be noticed at a glance by comparing spectra in Figure 1a,b, for instance, the absorption dips at low temperature result broader for NPs than the bulk correspondents. These general features are also observed in X-band spectra taken by a commercial spectrometer with 3D cavity (Supporting Information).

To appreciate differences and effects of nanostructuring, we parametrize the magnetization dynamics of single domain particle in the framework of the Landau–Lifshitz–Gilbert equation[20,21]

$$\frac{\partial \mathbf{M}}{\partial t} = \gamma_{\text{eff}} \left(\mathbf{M} \wedge \mathbf{B}_{\text{eff}} \right) + \alpha \frac{\gamma_{\text{eff}}}{M} \mathbf{M} \wedge \left(\mathbf{M} \wedge \mathbf{B}_{\text{eff}} \right) \quad (1)$$

where $\gamma_{\text{eff}} = g_{\text{eff}} \mu_B / \hbar$ is the effective gyromagnetic ratio. α is the Gilbert damping factor that can be ultimately associated with the spin–orbit coupling.[22] The effective field in each particle can be

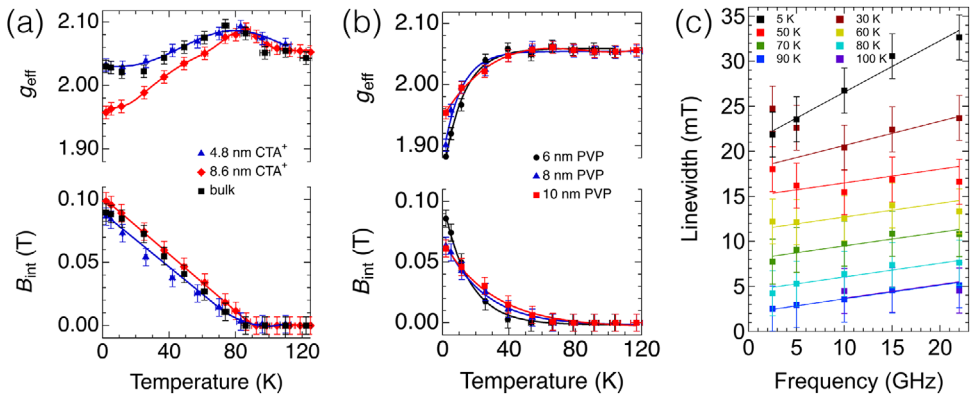

Figure 2. a,b) Temperature dependence of the effective *g*-factor and internal field as function of temperature. Lines are guides for the eyes. c) Frequency dependence of the HWHM linewidth extracted for 10 nm NPs in PVP. Solid lines display the trends obtained with Equation (3).

spelled out as:

$$B_{\text{eff}} = B_0 + B_{\text{MW}} + B_{\text{int}}$$

where B_0 is a static field, B_{MW} is the magnetic component of the electromagnetic field, $B_{\text{int}} = B_{\text{anis}} + B_{\text{demag}} + B_{\text{inter}}$ is the internal field which includes the anisotropy field B_{anis}, the demagnetizing field B_{demag} and the field B_{inter} generated by inter-particle dipolar or exchange interaction by neighboring NPs.

From previous studies, we expect that the magnetocrystalline anisotropy of CsNiCr NPs is related only to Ni(II) ions and it is estimated to be rather weak (0.5 kJ m^{-3}).[23] The surface anisotropy contribution is expected to represent the dominating term for small NPs, especially for 6 nm NPs where 40% of the atoms are located at the surface.[24] The demagnetizing field is expected to be more relevant for the smallest NPs due to their slightly elongated shape, while larger NPs have essentially cubic shape.[25] This term, however, is also affected by inter-particle dipolar interactions (B_{inter}) and thus strongly depends on the degree of dilution of the NPs in the non-magnetic matrix.[23]

The absorption dips observed in FMR spectra (Figure 1) occur when the precession of the magnetization **M** is resonant with B_{MW} at frequency ω_{res} while the line broadening is essentially given by the Gilbert damping term. For ferromagnetic systems with low anisotropy the resonance frequency of the FMR mode is expected to follow the Kittel formula,[20,26] that, for a powder, reads

$$\omega_{\text{res}} = \gamma_{\text{eff}} \left(B_0 + B_{\text{int}} \right) = \frac{g_{\text{eff}} \mu_{\text{B}}}{\hbar} \left(B_0 + B_{\text{int}} \right) \quad (2)$$

To track the evolution of the line position as a function of the different experimental parameters, we systematically measured the FMR spectra in frequency sweep mode and, from the measured transmission (S_{21}) spectra at increasing values of B_0, we evaluated the $\partial S_{21}/\partial B_0$ derivative and extracted the resonance frequency ω_{res} (see Figure S5, Supporting Information). By means of Equation (2), the effective *g*-factor (g_{eff}) and the internal field $B_{\text{int}} = B_{\text{anis}} + B_{\text{demag}} + B_{\text{inter}}$ have been subsequently extracted from the linear regression of the $\omega_{\text{res}}(B_0)$ dependence. The results are plotted as a function of temperature in **Figure 2**a,b. For all the samples, at 120 K, that is, in the paramagnetic phase, the effective *g*-factor is close to the average of the values $g_{\text{Ni}} = 2.15$ and $g_{\text{Cr}} = 1.99$ typically obtained for paramagnetic Ni(II) and Cr(III) ions. For bulk and for NP samples embedded in CTA$^+$, g_{eff} exhibits a maximum at $T \approx 90$ K (Figure 2a). B_{int} resulted vanishingly small for $T > 90$ K while a linear increase is observed below 90 K. This reveals, once more, the transition to ferromagnetic order at T_{C}. Note that, the temperature dependence of g_{eff} measured for 4.8 nm NPs in CTA$^+$ is closer to the bulk sample than that of 8.6 nm NPs. This is in line with the outcome of SANS measurements,[19] which have clearly pointed out the presence of inter-particle interactions B_{inter}. Thus we conclude that, for NP samples in CTA$^+$ matrix, B_{int} is dominated by B_{inter}, while B_{demag} is the mean demagnetizing field produced by clusters of NPs.

The temperature dependence of the g_{eff} and B_{int} parameters extracted for CsNiCr 10 nm NPs diluted in PVP polymer is shown in Figure 2b. In this case, the transition to the ferromagnetic ordered state is smoother and a downturn of g_{eff} versus T is observed below 60 K. This is also accompanied by a progressive increase of B_{int}, which exceeds 60 mT at 2 K. The same trend is obtained for NPs with higher dilution in PVP (see Supporting Information), suggesting that the temperature dependence of g_{eff} and B_{int} is not due to interparticle interactions or to macroscopic demagnetizing effects, pointing to negligible B_{inter} for PVP diluted samples. Similar behavior is observed in the temperature dependence of g_{eff} and B_{int} obtained for 6 and 8 nm NPs diluted in PVP (Figure 2b). Worth noting is the fact that size effects are evident only at the lowest temperature on the smallest (6 nm) NPs. It is also interesting to point out that, overall, $B_{\text{int}} \ll \omega_{\text{res}}/\gamma_{\text{eff}}$, while the relation $B_{\text{int}} \ll \mu_0 M_{\text{S}}$, where $M_{\text{s}} = 1.47 \times 10^5$ A m^{-1} is the saturation magnetization in the ordered phase, holds in the whole temperature range confirming the applicability of Equation (2) to describe the field dependence of ω_{res}[27,28] for all bulk and nanostructured samples.

The linewidth of field-swept FMR lines (Γ_{B}) is usually written as[20,29]

$$\Gamma_{\text{B}} = \Gamma_0 + \frac{\alpha}{2\gamma_{\text{eff}}}\omega \quad (3)$$

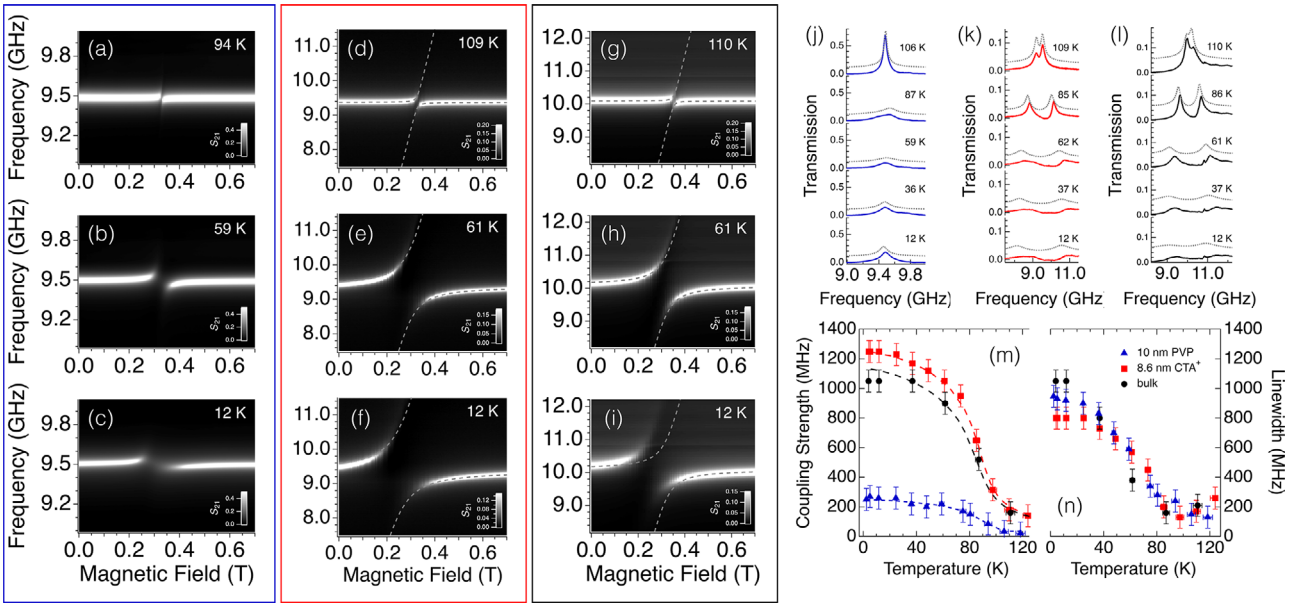

Figure 3. Transmission maps obtained at different temperature for a–c) 10 nm NPs in PVP; d–f) 8.6 nm NPs in CTA^+; g–i) bulk sample. Dashed lines show the calculated frequency dependence of the polariton branches. For each temperature, data are normalized to the maximum transmission. j–l) Transmission spectra taken at the resonance field respectively for 10 nm NPs in PVP, 8.6 nm NPs in CTA^+ and bulk. Dashed lines show the spectra calculated with the input–output formula (vertically shifted for clarity). For each sample and temperature, the line position is calculated with the effective *g*-factor and internal field parameters obtained from the FMR characterization. m,n) Temperature dependence of the extracted values of collective coupling strength and HWHM linewidth.

where the linear frequency dependence is related to the Gilbert damping factor (α) and Γ_0 is the zero-frequency offset, which is typically ascribed to sample inhomogeneities or to the presence of a distribution of local resonance fields across the sample.[29] To quantitatively evaluate the linewidth, we fitted the absorption dips shown in Figure 1a,b by means of a Lorentzian curve and extracted the half-width at half-maximum (HWHM) linewidth Γ_B. The values of Γ_B obtained for 10 nm NPs diluted in PVP are shown in Figure 2c. In the range 100 K < T < 60 K, the frequency dependence of Γ_B gives $\alpha = 0.0010 \pm 0.0005$, while at lower temperature the slope gets steeper and we obtained $\alpha = 0.0050 \pm 0.0005$ at 5 K. The increase of Γ_B upon cooling is also caused by larger Γ_0 values. This is compatible with the upturn of the internal field shown in Figure 2b, which may cause magnetic field inhomogeneity and broadening of the FMR line. Similar α behavior is also observed for NPs in PVP while a more complex temperature trend is shown by NPs in CTA^+ and by bulk samples. This is not surprising since these systems are more complex than a collection of single domain particles. Overall, the broadening of the FMR spectrum upon cooling is commonly observed in superparamagnetic NPs and typically ascribed to the progressive freezing of thermal fluctuations.[21] It is worth highlighting that the Gilbert damping coefficient $0.001 < \alpha < 0.005$ compares well with the values obtained for the lowest-order magnetostatic mode in YIG, which amounts to 2.3×10^{-4} for YIG micron-sized spheres,[30] but rises up to 0.03 for YIG nanoparticles.[31]

We now turn our attention to the coupling between the FMR mode and the cavity field. To this end, we used a planar microstrip resonator (see Experimental Section) with a large filling factor and resonance frequency ($\omega_c = 9.51$ GHz) matching the FMR mode of the CsNiCr samples in the presence of an applied magnetic field $B_{res} \approx 0.3$ T. **Figure 3** shows the evolution of the transmission maps in the 2–120 K temperature range for three different CsNiCr samples: 10 nm NPs in PVP, 8.6 nm NPs in CTA^+ and bulk. NPs of 10 nm size dispersed in PVP matrix behave as a collection of independent nanomagnets as discussed in the previous section. The spectral map in Figure 3a shows the presence of a small absorption dip that becomes progressively broader upon cooling (panels b and c). Conversely, transmission maps taken for $T \approx T_C$ on interacting NPs of 8.6 nm size in CTA^+ matrix (panels d–f) and on bulk samples (panels g–i) show the presence of an anticrossing, with double-peak spectra that are visible for $B = B_{res}$ (panels k and l). The evolution of the transmission maps as a function of temperature is similar for both 8.6 nm NPs in CTA^+ and bulk samples as it displays, in turns, a narrow anticrossing for $T \approx T_C$, the increase of the splitting upon cooling in the temperature range between 90 and 60 K and, last, a progressive decrease of the transmission of the two branches at lower temperatures (Figure 3d–i). The full data set with spectral maps acquired at several temperatures is reported in Supporting Information.

In the presence of a FMR mode with frequency ω_{res} given by Equation (2), the transmission of the resonator can be calculated by the input-output formula [32]

$$S_{21} = \frac{\kappa_{ext}}{i(\omega_c - \omega) + \left(\kappa_{ext} + \frac{1}{2}\kappa_{int}\right) + \frac{\Omega^2}{i(\omega_{res} - \omega) + \Gamma}} \quad (4)$$

where Ω is the spin–photon collective coupling strength, Γ is the half-width at half-maximum (HWHM) linewidth of the FMR line in frequency units and $\kappa = \kappa_{int} + \frac{\kappa_{ext}}{2}$ is the total loss of the

resonator given by the sum of the external (κ_{ext}) and internal (κ_{int}) contributions. The temperature dependence of the coupling strength is related to that of the magnetization $M(B_{res}, T)$ of the sample by

$$\Omega = \Omega_0 \sqrt{M\left(B_{res,}T\right)/M_s} \quad (5)$$

where Ω_0 is a constant and M_S is the magnetization at saturation.[33] In the strong coupling regime, which is characterized by $\Omega \gg (\Gamma, \kappa)$, the frequency dispersion of the two polaron branches can be reproduced by[34]

$$\omega_{\pm} = \omega_c + \frac{\Delta}{2} \pm \frac{\sqrt{\Delta^2 + 4\Omega^2}}{2} \quad (6)$$

where $\Delta = g_{eff}\mu_B(B - B_{res})/\hbar$.

For each temperature, we calculated the transmission maps with Equation (4) and we extracted the coupling and damping parameters that allowed us to reproduce the experimental data. The comparison between experiment and simulation is shown in Figure 3j–l for the spectra taken at $B = B_{res}$. The simulated transmission maps are reported in Supporting Information. The temperature dependence of Ω and Γ parameters obtained from simulations is shown in Figures 3m and 3n, respectively. For all samples, the increase of Ω between 120 and 60 K is related to the onset of the ferromagnetic transition in this temperature (and magnetic field) range. These trends are in perfect agreement with the behavior calculated by Equation (5) (dashed line) from the magnetization data (Supporting Information). For 10 nm NPs diluted in PVP polymer, the maximum value of the coupling strength resulted in Ω (2 K) $\approx$ 250 MHz. This value is much lower than those obtained for 8.6 nm NPs embedded in CTA^+ matrix and for the bulk sample, whose coupling strength exceeds 1000 MHz at low temperature. Straightforward explanation of this difference is the much larger density of spins in the latter and the presence of cooperative phenomena related to formation of clusters. The linewidth Γ follows, for the three samples, a similar temperature dependence with a progressive increase below 90 K upon cooling and values reaching 1000 MHz at 2 K. Concerning the damping rates of the microstrip resonator, the parameters extracted from simulations resulted in $16 < \kappa_{int} < 26$ MHz and $\kappa_{ext} \ll \kappa_{int}$, thus $\Gamma \gg \kappa$. Simulations with Equation (5) evidence that such a large difference between κ and the values of Γ and Ω accounts for the weak transmission measured at low temperature for the polaron branches.

In summary, we studied the evolution of the FMR mode on bulk and nanostructured CsNiCr samples under the effects of different experimental parameters, including temperature, microwave frequency, NP size and dispersion in different non-magnetic matrices. A Gilbert damping parameter of 10^{-3} is extracted from the frequency dependence of the linewidth measured for isolated 10 nm size NPs. The coupling between CsNiCr samples and the microwave field has been investigated by means of a planar microstrip resonator. Clear differences emerge between the behavior of magnetically isolated NPs in PVP polymer and mutually interacting NPs embedded in CTA^+ matrix or the bulk sample. For 6 and 10 nm size NPs diluted in PVP polymer the condition $\Omega < \Gamma$ holds in the whole temperature range, clearly indicating the presence of weak coupling between spins and photons. Conversely, for 4.8 and 8.6 nm size NPs embedded in CTA^+ matrix, as well as for the bulk sample, the condition $\Omega > \Gamma$ holds for $T < 110$ K, evidencing the achievement of the strong coupling regime at temperature close and below T_C. With these numbers, the cooperativity, that is, $C = \Omega/\kappa\Gamma$, results C (97 K) = 29.3 and C (4 K) = 100.2 for 8.6 nm NPs in CTA^+. Overall, the strong coupling between bulk or nanostructured CsNiCr Prussian blue analogue and the cavity field of a planar resonator follows as a consequence of the large collective coupling that exceeds the damping of the FMR mode. These results clarify conditions for the coherent manipulation of collective spin degrees of freedom in nanostructured coordination materials and open up new possibilities for the exploitation of nanostructured coordination materials in the field of quantum magnonics and spintronics.

Experimental Section

CsNiCr nanoparticles embedded in PVP and CTA^+ matrices were prepared following ref. 35: a relatively diluted aqueous solution of $K_3[Cr(CN)_6]$ (c = 1 mM L^{-1}) was added to an aqueous solution containing $NiCl_2$, $6H_2O$ (c = 1 mM L^{-1}) and 2 molar equivalents of CsCl. A light green solution was obtained. Dynamic Light Scattering (DLS) measurements performed after 1 h reveals a size of 6–7 nm including the solvation shell. Scanning transmission electronic microscopy (STEM) observations showed objects with a size of around 5 nm. The zeta potential was measured for these particles to be $z = -31$ mV evidencing their negative charge (the counter cation being Cs^+). In order to prepare particles with larger sizes, that is, around 8 and 10 nm, the 6 nm pristine particles were used as seeds and the two precursors ($K_3[Cr(CN)_6]$ and $NiCl_2$,$6H_2O$) were added simultaneously to the dispersion as already described.[36] The reaction was stopped when the exact amount of precursors corresponding to the targeted size was added. The particles were recovered by two different methods: i) after 1 h reaction, the organic polymer polyvinylpyrrolidone (PVP) was introduced with a [monomer]/[Ni^{2+}] ratio of 300 and then acetone was added to obtain a precipitate containing the nanoparticles coated with PVP and ii) after 1 h reaction, 3 molar equivalents of cetyl trimethyl ammonium chloride (CTACl) were added, which leads to the precipitation of the particles. It is worth noting that, here, the CTA^+ plays both the role of counter cation and organic surfactant of the negatively charged particles.

The "bulk" sample was obtained by mixing *concentrated* aqueous solutions (10 mM L^{-1}) of the two precursors, which leads to the precipitation of the micron-sized aggregates of CsNiCr as described in ref. 15. In all cases, X-ray powder diffraction studies showed the presence of the patterns expected for the face centered cubic structure of the particles with different sizes of 6, 8, 10 nm and larger than a micron for the "bulk" like sample.

Transmission spectroscopy data were acquired out by means of a Vector Network Analyzer in the 1–26 GHz range. These experiments were carried out in a Quantum Design PPMS by means of a home-made insert wired with two coaxial lines.[37] Broadband measurements were performed with a 500 μm wide continuous microstrip, while half-wavelength microstrip resonators were obtained by means of a 5.5 mm long metal strip separated from the feedlines by two 300 μm wide coupling gaps.[37] Planar devices were fabricated by optical lithography and wet etching in NH_4:H_2O_2 (9:1) aqueous solution of thermally evaporated Ag (3 μm)/Ti (10 nm)/sapphire (460 μm) films.

The transmission spectrum of the bare microstrip resonator measured at 2 K and in zero applied magnetic field is shown in Supporting Information. Curve fitting of the $S_{21}(\omega)$ dependence with a conventional quasi-Lorentzian lineshape provides resonance frequency $\omega_c / 2\pi = 9.51$ GHz, loaded quality factor $Q = 635$ and insertion loss IL = 16.2 dB.

CsNiCr NPs and bulk samples were pressed to form a cylinder-shaped pellet (base diameter 5 mm), which were attached in the middle of the

microstrip by means of a thin layer of silicone grease. The height of the sample is typically ≈2 mm.

Supporting Information

Supporting Information is available from the Wiley Online Library or from the author.

Acknowledgements

This work was supported by the U.S. Air Force Office of Scientific Research (AOARD) under award number FA2386-17-1-4040.

Conflict of Interest

The authors declare no conflict of interest.

Keywords

coherent spin–photon coupling, coordination nanoparticles, ferromagnetic resonance, magnonics, Prussian blue analogues

Received: August 19, 2019
Revised: October 29, 2019
Published online:

[1] C. W. Sandweg, Y. Kajiwara, A. V. Chumak, A. A. Serga, V. I. Vasyuchka, M. B. Jungfleisch, E. Saitoh, B. Hillebrands, *Phys. Rev. Lett.* **2011**, *106*, 216601.
[2] K. Uchida, S. Takahashi, K. Harii, J. Ieda, W. Koshibae, K. Ando, S. Maekawa, E. Saitoh, *Nature* **2008**, *455*, 778.
[3] G. E. W. Bauer, A. H. MacDonald, S. Maekawa, *Solid State Commun.* **2010**, *150*, 459.
[4] O. Rousseau, B. Rana, R. Anami, M. Yamada, K. Miura, S. Ogawa, Y. Otani, *Sci. Rep.* **2015**, *5*, 9873.
[5] A. Khitun, M. Bao, K. L Wang, *J. Phys. D: Appl. Phys.* **2010**, *43*, 264005.
[6] G. Kurizki, P. Bertet, Y. Kubo, K. Mølmer, D. Petrosyand, P. Rabl, J. Schmiedmayer, *Proc. Natl. Acad. Sci. USA* **2015**, *112*, 3866.
[7] D. Lachance-Quirion, Y. Tabuchi, A. Gloppe, K. Usami, Y. Nakamura, *Sci. Adv.* **2017**, *3*, e1603150.
[8] V. Cherepanov, I. Kolokolov, V. L'vov, *Phys. Rep.* **1993**, *229*, 81.
[9] A. A. Serga, A. V. Chumak, B. Hillebrands, *J. Phys. D: Appl. Phys.* **2010**, *43*, 264002.
[10] H. Liu, Chuang Zhang, H. Malissa, M. Groesbeck, M. Kavand, R. McLaughlin, S. Jamali, J. Hao, D. Sun, R. A. Davidson, L. Wojcik, J. S. Miller, C. Boehme, Z. V. Vardeny, *Nat. Mater.* **2018**, *17*, 308.
[11] M. Verdaguer, G. S. Girolami, in *Magnetism: Molecules to Materials V*, (Eds: J. S. Miller, M. Drillon), Wiley-VCH, Weinheim, Germany **2005**.
[12] M. Pregelj, A. Zorko, D. Arčon, S. Margadonna, K. Prassides, H. van Tol, L. C. Brunel, O. Ozarowski, *J. Magn. Magn. Mater.* **2007**, *316*, e680.
[13] Á. Antal, A. Jánossy, L. Forró, E. J. M. Vertelman, P. J. van Koningsbruggen, P. H. M. van Loosdrecht, *Phys. Rev. B* **2010**, *82*, 014422.
[14] D. M. Pajerowski, J. E. Gardner, M. J. Andrus, S. Datta, A. Gomez, S. W. Kycia, S. Hill, D. R. Talham, M. W. Meisel, *Phys. Rev. B* **2010**, *82*, 214405.
[15] V. Gadet, T. Mallah, I. Castro, M. Verdaguer, P. Veillet, *J. Am. Chem. Soc.* **1992**, *114*, 9213.
[16] Y. Prado, L. Lisnard, D. Heurtaux, G. Rogez, A. Gloter, O. Stephan, N. Dia, E. Riviere, L. Catala, T. Mallah, *Chem. Commun.* **2011**, *47*, 1051.
[17] L. Catalá, T. Mallah, *Coord. Chem. Rev.* **2017**, *346*, 32.
[18] K. Ridier, B. Gillon, G. André, G. Chaboussant, L. Catala, S. Mazérat, T. Mallah, *J. Appl. Phys.* **2015**, *118*, 114304.
[19] K. Ridier, B. Gillon, G. Chaboussant, L. Catala, S. Mazérat, E. Rivière, T. Mallah, *Eur. Phys. J. B* **2017**, *90*, 77.
[20] S. V. Vonsovskii, *Ferromagnetic Resonance*, Pergamon, Oxford **1966**.
[21] J. Kliava, in *Magnetic Nanoparticles* (Ed: S. P. Gubin), Wiley-VCH, Weinheim, Germany **2009**.
[22] M. C. Hickey, J. S. Moodera, *Phys. Rev. Lett.* **2009**, *102*, 137601.
[23] Y. Prado, S. Mazerat, E. Rivière, G. Rogez, A. Gloter, O. Stéphan, L. Catala, T. Mallah, *Adv. Funct. Mater.* **2014**, *24*, 5402.
[24] Y. Prado, M.-A. Arrio, F. Volatron, E. Otero, C. Cartier dit Moulin, P. Sainctavit, L. Catala, T. Mallah, *Chem. - Eur. J.* **2013**, *19*, 6685.
[25] L. Catala, A. Gloter, O. Stephan, G. Rogez, T. Mallah, *Chem. Commun.* **2006**, 1018.
[26] C. Kittel, *Phys. Rev.* **1948**, *73*, 155.
[27] E. Schlomann, J. R. Zeender, *J. Phys. Chem.* **1958**, *6*, 257.
[28] R. S. de Biasi, T. C. Devezas, *J. Appl. Phys.* **1978**, *49*, 2466.
[29] A. Barman, J. Sinha, *Spin Dynamics and Damping in Ferromagnetic Thin Films and Nanostructures*, Springer, Cham, Switzerland **2018**.
[30] a) H. Huebl, C. W. Zollitsch, J. Lotze, F. Hocke, M. Greifenstein, A. Marx, R. Gross, S. T. B. Goennenwein, *Phys. Rev. Lett.* **2013**, *111*, 127003; b) Y. Tabuchi, S. Ishino, T. Ishikawa, R. Yamazaki, K. Usami, Y. Nakamura, *Phys. Rev. Lett.* **2014**, *113*, 083603; c) X. Zhang, C.-L. Zou, L. Jiang, H. X. Tang, *Phys. Rev. Lett.* **2014**, *113*, 156401; d) X. Zhang, C.-L. Zou, N. Zhu, F. Marquardt, L. Jiang, H. X. Tang, *Nat. Commun.* **2015**, *6*, 8914; e) X. Zhang, C.-L. Zou, L. Jiang, H. X. Tang, *Sci. Adv.* **2016**, *2*, e1501286; f) N. Kostylev, M. Goryachev, M. E. Tobar, *Appl. Phys. Lett.* **2016**, *108*, 062402; g) R. G. E. Morris, A. F. van Loo, S. Kosen, A. D. Karenowska, *Sci. Rep.* **2017**, *7*, 11511.
[31] V. Sharma, J. Saha, S. Patnaik, B. K. Kuanr, *J. Magn. Magn. Mater.* **2017**, *439*, 277.
[32] C. Bonizzoni, A. Ghirri, M. Atzori, L. Sorace, R. Sessoli, M. Affronte, *Sci. Rep.* **2017**, *7*, 13096.
[33] A. Ghirri, C. Bonizzoni, F. Troiani, N. Buccheri, L. Beverina, A. Cassinese, M. Affronte, *Phys. Rev. A* **2016**, *93*, 063855.
[34] A. Ghirri, C. Bonizzoni, D. Gerace, S. Sanna, A. Cassinese, M. Affronte, *Appl. Phys. Lett.* **2015**, *106*, 184101.
[35] D. Brinzei, L. Catala, N. Louvain, G. Rogez, O. Stéphan, A. Gloter, T. Mallah, *J. Mater. Chem.* **2006**, *16*, 2593.
[36] L. Catala, D. Brinzei, Y. Prado, A. Gloter, O. Stéphan, G. Rogez, T. Mallah, *Angew. Chem., Int. Ed.* **2009**, *48*, 183.
[37] A. Ghirri, C. Bonizzoni, M. Righi, F. Fedele, G. Timco, R. Winpenny, M. Affronte, *Appl. Magn. Reson.* **2015**, *46*, 749.

